

# Hydrodynamic Self-Consistent Field Theory for Inhomogeneous Polymer Melts

David M. Hall,<sup>1,2</sup> Turab Lookman,<sup>2</sup> Glenn H. Fredrickson,<sup>3,4</sup> and Sanjoy Banerjee<sup>4</sup>

<sup>1</sup> Department of Physics, University of California Santa Barbara, Santa Barbara, CA 93106

<sup>2</sup> Los Alamos National Laboratory, Theoretical Division, Los Alamos, NM 87545

<sup>3</sup> Materials Research Laboratory, University of California Santa Barbara, Santa Barbara, CA 93106

<sup>4</sup> Department of Chemical Engineering, University of California Santa Barbara, Santa Barbara, CA 93106

(Dated: December 2, 2024)

We introduce a mesoscale technique for simulating the structure and rheology of block copolymer melts and blends in hydrodynamic flows. This technique is an extension of dynamic self consistent field theory (DSCFT) that allows for hydrodynamic flow in channels with arbitrarily complex geometries. We demonstrate the technique by examining an ABC triblock copolymer melt and a ternary (A+B+C) homopolymer blend flowing within straight and constricted channels. We observe that the walls produce microphase alignment through the action of boundary wetting forces at the wall-melt interface and by inducing shearing flows. In the case of the triblock melt, these two effects compete, producing wall normal alignment in the no flow case and wall parallel alignment for a flowing melt.

Inhomogeneous polymer formulations play an important role in existing and future applications including paints, adhesives, organic electronics, advanced plastics, personal care products, cosmetics, and processed foods. Many of these systems are structured on length scales spanning nanometers to millimeters and the stabilization of the finest scale fluid structures is often assisted by the presence of block or graft copolymer components [1]. To date, most polymer formulations have been arrived at by trial and error experimentation which is time consuming and expensive. Ideally, numerical techniques can be used to explore the large design space in a more cost-effective manner, and computational tools [2, 3, 4] have been constructed that can predict equilibrium properties of polymeric materials as a function of their composition and architecture variables. However, prediction of equilibrium properties represents only the first step in designing new formulations as most real-world products exist in non-equilibrium states that are kinetically trapped when quenched to room temperature. In such non-equilibrium states, bulk properties such as strength, optical clarity, and elasticity depend in detail on the size and distribution of the inhomogeneities, which in turn are determined by the composition of the fluid state and the manner in which the fluid was processed.

An accurate simulation of realistic polymeric fluids in industrial processes involves a host of technically challenging phenomena including viscoelastic turbulence, glass formation, viscous heating, dynamic asymmetry between components, the presence of impurities, and many others. Although we cannot tackle all of these challenges simultaneously, we begin by constructing a technique that captures the fundamentals of self assembly, convective transport, and polymer viscoelasticity. Our scheme employs a non-equilibrium version of self consistent field theory (SCFT) that models material specific self assembly of block copolymers [4]. This thermodynamic model

is then coupled to a multiple fluid hydrodynamic model to simulate convective transport of conserved quantities and to a set of constitutive equations that describe viscoelastic stresses in an entangled polymer melt. In addition to the usual concentration fields, the SCFT model and the multi-fluid model contain a set of continuous wall fields representing the presence of a rigid porous material that can be shaped to form channel walls with complex geometries. These walls can be fixed or moving on a predetermined path, simulating the interaction of machinery with the melt at micro-fluidic scales.

Our technique is an extension of self consistent field theory to non-equilibrium states, and therefore it is related to other dynamic self consistent field theory (DSCFT) schemes [5, 6, 7, 8, 9, 10]. However, our scheme represents a significant advance over previous approaches in that it incorporates full hydrodynamics and is capable of simulating flows in arbitrarily complex channel geometries. This technique also represents an advance over “phase field” hydrodynamic schemes that employ a Ginzburg-Landau (GL) free energy [11, 12], in that it captures architecture-specific self assembly in block copolymers and copolymer blends. Subsequently, we refer to our scheme as hydrodynamic self consistent field theory (HSCFT) to underscore its emphasis on hydrodynamic transport.

In this letter, we introduce a viscoelastic multiple-fluid model for block copolymers and melt blends and we outline the dynamic SCFT model used to capture material specific properties in the presence of rigid channel walls. We then apply this technique to examine the flow of an ABC triblock melt and a three component homopolymer blend in a straight channel and in a channel with a narrow constriction.

Our system is composed of a blend of  $C$  distinguishable copolymer species each of which contains  $M_\alpha^\phi$  distinct monomers, where  $\alpha \in \{1\dots C\}$ . The system con-

tains  $n_\alpha^\phi$  copies of each copolymer with polymerization index  $N_\alpha$  and entanglement length  $N_{e\alpha}$ . There are also  $M^\psi$  distinguishable mesoscale wall units of which there are  $n_j^\psi$  each, where  $j \in \{1 \dots M^\psi\}$  in a system of volume  $V$ . Each mesoscale unit is taken to occupy an equal volume in the melt  $v_0 = V / (\sum_\alpha n_\alpha^\phi \bar{N} + \sum_j n_j^\psi)$ , where  $\bar{N} = \sum_\alpha n_\alpha^\phi N_\alpha / \sum_\beta n_\beta^\phi$  is the average index of polymerization.

Following [13], we derived a multiple-fluid model that tracks the transport of an arbitrary number of viscoelastic fluids at zero Reynolds number. The monomer volume fraction fields  $\phi_{\alpha i}$  are transported with total velocity  $\mathbf{v}_{\alpha i}^\phi$  by Eq. (1), and the wall volume fractions  $\psi_j$  are transported with total velocity  $\mathbf{v}_j^\psi$  by Eq. (2).

$$\partial_t \phi_{\alpha i} = -\nabla \cdot \phi_{\alpha i} \mathbf{v}_{\alpha i}^\phi \quad (1)$$

$$\partial_t \psi_j = -\nabla \cdot \psi_j \mathbf{v}_j^\psi \quad (2)$$

$$\mathbf{w}_{\alpha i}^\phi = \frac{1}{\zeta_{\alpha i}^\phi} \left[ \alpha_{\alpha i}^\phi \nabla \cdot \boldsymbol{\sigma} - \phi_{\alpha i} \nabla \mu_{\alpha i}^\phi - \phi_{\alpha i} \nabla p + \phi_{\alpha i} \mathbf{f}_e \right] \quad (3)$$

$$\mathbf{f}_j^\psi = \psi_j \nabla \mu_j^\psi + \psi_j \nabla p - \alpha_j^\psi \nabla \cdot \boldsymbol{\sigma} + \zeta_j^\psi (\mathbf{v}_j^\psi - \mathbf{v}_T) \quad (4)$$

$$0 = \nabla \pi + \nabla p - \nabla \cdot \boldsymbol{\sigma} - \mathbf{f}^\psi - \mathbf{f}^\phi \quad (5)$$

The monomer velocities can be split into two parts  $\mathbf{v}_{\alpha i}^\phi = \mathbf{v}_T + \mathbf{w}_{\alpha i}^\phi$ . The first part  $\mathbf{v}_T = \sum_{\alpha i} \alpha_{\alpha i}^\phi \mathbf{v}_{\alpha i}^\phi + \sum_j \alpha_j^\psi \mathbf{v}_j^\psi$  is called the tube velocity and represents the rheological mean velocity, as weighted by the stress division parameters  $\alpha_{\alpha i}^\phi = \zeta_{\alpha i}^\phi / \zeta$  and  $\alpha_j^\psi = \zeta_j^\psi / \zeta$  (where we use the shorthand notation  $\sum_{\alpha i} = \sum_{\alpha=1}^C \sum_{i=1}^{M_\alpha^\phi}$ ). The second part  $\mathbf{w}_{\alpha i}^\phi$  represents the velocity of each component relative to  $\mathbf{v}_T$ . The stress division parameters are defined in terms of  $\zeta = \sum_{\alpha i} \zeta_{\alpha i}^\phi + \sum_j \zeta_j^\psi$  where the friction coefficients are assumed to have the form  $\zeta_{\alpha i}^\phi = \frac{1}{v_0} \zeta_{0i}^\phi \phi_{\alpha i} N_\alpha / N_{e\alpha}$  and  $\zeta_j^\psi = \frac{1}{v_0} \zeta_{0j}^\psi \psi_j / \Phi$  and the porosity of the solid wall is  $\Phi = 1 - \sum_j \psi_j$ . The quantities  $\zeta_{0i}^\phi$  and  $\zeta_{0j}^\psi$  are single-monomer friction coefficients.

Relative flows  $\mathbf{w}_{\alpha i}$  are produced as a result of imbalanced osmotic forces  $\phi_{\alpha i} \nabla \mu_{\alpha i}$ , pressure gradients, viscoelastic forces  $\nabla \cdot \boldsymbol{\sigma}$ , and the influence of an external bulk force (such as gravity)  $\mathbf{f}_e$  as described by Eq. (3).

The wall velocity fields  $\mathbf{v}_j^\psi$  are externally constrained to impart a predetermined path to each solid object. By inserting them into Eq. (4), we can compute the local wall forces  $\mathbf{f}_j^\psi$  required to achieve this motion, and by integrating these forces over an entire solid object, we can measure the net force and torque experienced by that object.

Cooperative flows are produced that balance the total osmotic force  $\nabla \pi = \sum_{\alpha i} \phi_{\alpha i} \nabla \mu_i^\phi + \sum_j \psi_j \nabla \mu_j^\psi$ , the hydrodynamic pressure gradients  $\nabla p$ , the viscoelastic forces  $\nabla \cdot \boldsymbol{\sigma}$ , the wall forces  $\mathbf{f}^\psi$ , and the bulk forces acting on the melt  $\mathbf{f}^\phi$  as shown in Eq. (5). The sum of all wall forces acting on the melt is  $\mathbf{f}^\psi = \sum_j \mathbf{f}_j^\psi$  and similarly, the total bulk force on the melt is  $\mathbf{f}^\phi = \sum_{\alpha i} \mathbf{f}_{\alpha i}^\phi = \mathbf{f}_e \Phi$ . The mean

velocity  $\mathbf{v} = \sum_{\alpha i} \phi_{\alpha i} \mathbf{v}_{\alpha i}^\phi + \sum_j \psi_j \mathbf{v}_j^\psi$  and pressure fields  $p$  must simultaneously satisfy this force balance condition Eq. (5) while conserving mass  $\nabla \cdot \mathbf{v} = 0$ . Since these relationships are not easily inverted, we solve them using an iterative procedure. Once we have obtained  $\mathbf{v}$  and  $\mathbf{w}_j^\phi$ , the tube velocity can be calculated.

$$\mathbf{v}_T = \frac{\sum_{\alpha i} (\alpha_{\alpha i}^\phi - \phi_{\alpha i}) \mathbf{w}_{\alpha i}^\phi + \sum_j (\alpha_j^\psi - \psi_j) \mathbf{v}_j^\psi + \mathbf{v}}{1 - \sum_{\alpha i} (\alpha_{\alpha i}^\phi - \phi_{\alpha i})} \quad (6)$$

The constitutive equations (7) and (8) measure the bulk elastic stresses  $\boldsymbol{\sigma}_{\alpha i}^b$  and shear elastic stresses  $\boldsymbol{\sigma}_{\alpha i}^s$  induced by deformations of each entangled polymeric component.

$$\boldsymbol{\sigma}_{\alpha i}^s = G_{\alpha i} \kappa_T - \boldsymbol{\sigma}_{\alpha i}^s / \tau_\alpha \quad (7)$$

$$\boldsymbol{\sigma}_{\alpha i}^b = K_{\alpha i} (\nabla \cdot \mathbf{v}_T) \boldsymbol{\delta} - \boldsymbol{\sigma}_{\alpha i}^b / \tau_\alpha \quad (8)$$

Although there are many possible constitutive equations, we have chosen to employ the Oldroyd-B model in which the total viscoelastic force is produced by the sum of the elastic forces contributed by each polymeric component and a dissipative viscous force,  $\nabla \cdot \boldsymbol{\sigma} = \sum_{\alpha i} (\nabla \cdot \boldsymbol{\sigma}_{\alpha i}^s + \nabla \cdot \boldsymbol{\sigma}_{\alpha i}^b) + \eta_s \nabla^2 \mathbf{v}_T$ . This model allows us to study a purely viscous fluid ( $G_{\alpha i} = K_{\alpha i} = 0$ ), a purely viscoelastic melt ( $\eta_s = 0$ ), or anything in-between. The derivatives in (7) and (8) are upper convected time derivatives,  $\dot{\boldsymbol{\sigma}} = \partial_t \boldsymbol{\sigma} + \mathbf{v}_T \cdot \nabla \boldsymbol{\sigma} - \boldsymbol{\sigma} \cdot \nabla \mathbf{v}_T - (\nabla \mathbf{v}_T)^\dagger \cdot \boldsymbol{\sigma}$ , and the shear strain rate tensor is  $\kappa_T^{ij} = \partial_i v_T^j + \partial_j v_T^i - \frac{2}{d} (\nabla \cdot \mathbf{v}_T) \delta_{ij}$ . The concentration dependent bulk moduli  $K_{\alpha i}$  and shear moduli  $G_{\alpha i}$  measure stresses imposed on a single component by the applied strains. Following Tanaka's example [12], we employ moduli of the form  $G_{\alpha i}(\phi) = G_{0\alpha i} \phi_{\alpha i}^2$  and  $K_{\alpha i}(\phi) = K_{0\alpha i} \theta(\phi_{\alpha i} - f_{\alpha i})$  where  $\theta$  is the Heaviside step function. For simulations with large elastic strains, this constitutive equation can be replaced with a more sophisticated phenomenological model or one based upon the SCFT microphysics [14].

An SCFT calculation produces the chemical potential gradients that drive the phase separation processes. The free energy of the melt is  $F = U - TS$  where the enthalpy is given by

$$U/kT = \frac{1}{v_0 \bar{N}} \int d\mathbf{r} \left[ \frac{1}{2} \sum_{\alpha, i, \beta, j} \phi_{\alpha i} \bar{N} \chi_{\alpha i \beta j}^\phi \phi_{\beta j} + \sum_{i, \beta, j} \psi_i \bar{N} \chi_{i \beta j}^\psi \phi_{\beta j} \right] \quad (9)$$

The  $\chi^\phi$  and  $\chi^\psi$  denote segment-segment and segment-wall interactions, respectively, and the entropy is

$$S/k = \sum_\alpha n_\alpha^\phi \ln Q_\alpha + \frac{1}{v_0 \bar{N}} \int d\mathbf{r} \sum_{\alpha, i} \omega_{\alpha i}^\phi \phi_{\alpha i} \quad (10)$$

The quantity  $Q_\alpha[\omega]$  is the partition function over all configurations of a single copolymer species  $\alpha$  in the presence of the fields  $\omega_{\beta i}^\phi$ .

Traditional SCFT models assume that all fields are held in equilibrium. Dynamic SCFT models rely instead on the fact that system variables can be separated into two sets which relax on widely separated time scales. Here we assume that all fluid degrees of freedom other than those manifestly treated by the theory are “fast” relaxing variables that remain at local equilibrium. The slow variables include the elastic network stresses and conserved quantities such as mass, momentum, and monomer number. Other variables, such as the conjugate chemical fields  $\omega_{\alpha i}^\phi$  are fast relaxing parameters, held in local equilibrium. We compute the fast set of parameters by numerically solving the local thermodynamic equilibrium (LTE) conditions [14]  $\tilde{\phi}_{\alpha i}[\omega] = \phi_{\alpha i}$ , which are derived by extremizing the free energy with respect to the equilibrated fields  $\omega_{\alpha i}^\phi(\mathbf{r})$ . The volume fraction fields  $\phi_{\alpha i}$  and  $\psi_j$  are not in local equilibrium and give rise to imbalanced chemical potentials  $\mu_{\alpha i}^\phi(\mathbf{r}) = \frac{\delta F}{\delta \phi_{\alpha i}(\mathbf{r})} = \frac{kT}{Nv_0} \left[ \sum_{\beta j} \bar{N} \chi_{\alpha i \beta j}^\phi \phi_{\beta j} + \sum_k \bar{N} \chi_{k \alpha i}^\psi \psi_k - \omega_{\alpha i}^\phi \right]$  and  $\mu_i^\psi(\mathbf{r}) = \frac{\delta F}{\delta \psi_i(\mathbf{r})} = \frac{kT}{Nv_0} \sum_{\beta j} \bar{N} \chi_{i \beta j}^\psi \phi_{\beta j}$  that drive diffusion and phase separation.

Calculations are performed in a periodic cell in two or three dimensions and non-periodic channel geometries are approximated by employing an appropriate distribution of rigid materials. Spatial derivatives are computed pseudo-spectrally in Fourier space which enables us to resolve sharp domain interfaces with a small number of grid points and lends itself readily to parallelization.

The multi-fluid model is solved using a pseudo-time iteration, which begins by estimating  $\boldsymbol{\sigma}, \mathbf{w}$  and  $\mathbf{f}^\psi$  using  $\mathbf{v}$  and  $p$  fields from the previous iteration. Then new pressure and velocity fields are calculated using a projection method and a flow penalization technique at the walls. This procedure repeats until a pseudo-steady state is achieved that satisfies the no-flow and no-slip boundary conditions as well as incompressibility ( $\nabla \cdot \mathbf{v} = 0$ ) and the zero Reynolds number force balance condition (5). The new velocity fields are then used to transport the volume fraction fields.

Similarly, the SCFT model iterates to find chemical potentials  $\mu$  that satisfy the LTE conditions. The conjugate potential fields  $\omega$  are used to calculate auxiliary monomer volume fractions, and residual errors are reduced using a hill-climbing technique. Line minimization in the current search direction speeds convergence.

We illustrate our scheme by studying the dynamics and structural evolution of two representative systems in two channel configurations, namely an ABC triblock copolymer melt and an A+B+C three component homopolymer blend in a straight channel and in a channel with a narrow constriction. Each system consists of an incompressible melt that has been quenched from a disordered state into the intermediate segregation regime. Hydrodynamic motion is produced as a result of internal thermodynamic forces driving incompatible components

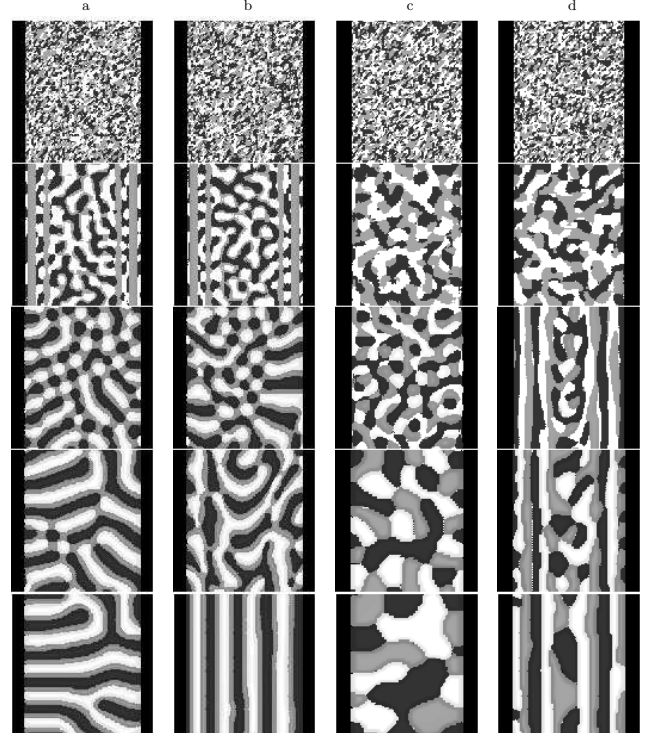


FIG. 1: Time evolution of a quenched triblock melt and a quenched three component homopolymer blend in a straight channel. Time increases from top to bottom. (a) Stationary triblock melt  $Wi = 0.006$  (b) Triblock melt with bulk flow from top to bottom  $Wi = 0.161$ . (c) Stationary blend  $Wi = 0.004$  (d) Blend with bulk flow from top to bottom  $Wi = 0.171$

to phase separate and by the bulk transport of materials due to the externally applied force field  $\mathbf{f}_e$ .

In both systems, each component occupies an equal volume fraction in the melt,  $f_A = f_B = f_C$ . The left two sequences (a) and (b) illustrate the evolution of a triblock ( $\chi_{\alpha i \beta j}^\phi = 25$ ,  $\chi_{i \beta j}^\psi = 12$ ) with and without bulk flow, and the right two sequences (c) and (d) correspond to a three component blend ( $\chi_{\alpha i \beta j}^\phi = \chi_{i \beta j}^\psi = 12$ ) with and without bulk flow. The remaining system parameters were chosen to approximate a polystyrene melt, with  $\zeta_0 = 10^{-8}$  Ns/m and  $G_0 = 2000$  kPa [15]. The flow rates are characterized by the maximum Weissenburg number  $Wi = \tau v_{\max} / L$  where  $v_{\max}$  is the maximum mean velocity. For the straight pipe the characteristic width is the channel diameter  $L = D$  and for the constricted pipe, we use the constriction diameter  $L = d$  (where  $d = 0.2D$ ).

In Fig. 1 we examine the behavior of a triblock melt and a three component homopolymer blend confined to a smooth pipe. Sequences (a) and (c) illustrate the evolution of these systems in the presence of neutral channel walls without bulk flow ( $\mathbf{f}_e = 0$ ). At early times the tri-blocks develop short lived structures parallel to the walls due to dynamic asymmetry between the central block and the end blocks. Fluctuations in the end-blocks grow

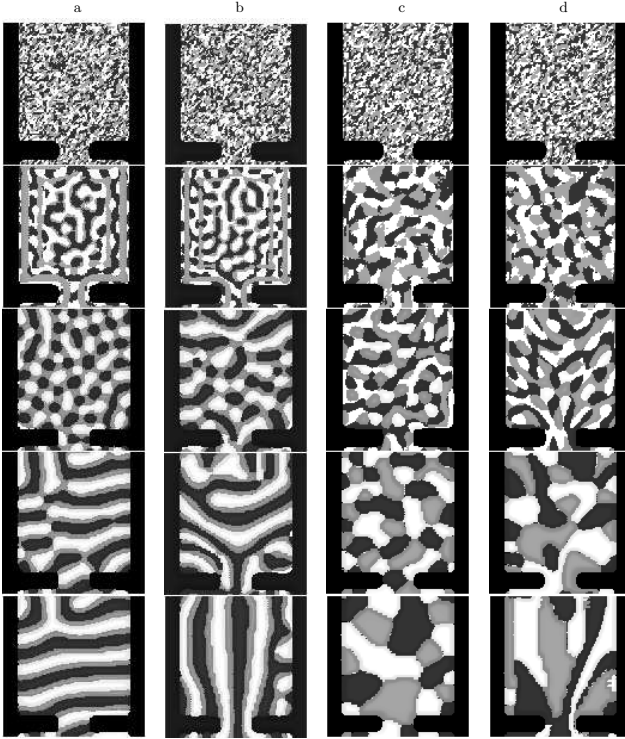


FIG. 2: Time evolution of a triblock melt and three component homopolymer blend in a channel with a narrow constriction. (a) Stationary triblock melt  $Wi = 0.024$  (b) Triblock melt with bulk flow from top to bottom  $Wi = 0.205$  (c) Stationary blend  $Wi = 0.013$  (d) Blend with bulk flow from top to bottom  $Wi = 0.206$

more quickly, resulting in a region of enhanced A and C monomers near the wall, with a region of enhanced B monomers beside it. After the fluctuations saturate, lamellar micro-domains locally arrange themselves in a perpendicular configuration relative to the wall. This behavior is not present in the stationary blend.

When we apply a nonzero forcing field ( $\mathbf{f}_e \neq 0$ ), it produces a pressure driven flow in the melt. In a straight pipe such as that in Fig. 1, the boundaries produce an approximate parabolic velocity profile with the largest shear stresses at the walls. The shear is sufficient to align the triblock lamellae (b) in a wall-parallel configuration near the walls which induces a wall parallel configuration in the low shear regions as well. In the A+B+C blend, wall parallel configurations are produced in the high shear regions near the wall.

We examine the behavior of these same materials in an extrusive flow in which shear, extensional, and rotational stresses are present, by adding a narrow constriction to the channel. Comparing Fig. 2 with Fig. 1 demonstrates how the constriction modifies the flow. As before, the tri-block systems (a) and (b) develop layers of enhanced B block that mirror the channel contours in the early stages of phase separation, and the stationary triblock melt (a) develops wall perpendicular lamellae at late times with

distortion around the constriction. As in the straight pipe, when a pressure driven flow is applied the triblock melt aligns itself with the flow (b), although the constriction delays the onset of this steady state configuration.

The constriction has little effect on the stationary blend (c), as it is indifferent to the neutral walls, but flow introduces two competing effects in the extruded blend (d). It speeds phase separation after saturation by relaxing kinetically trapped states, but the constriction creates a velocity field that tends to rupture domains and slow coarsening.

To summarize, we have developed a new type of dynamic self consistent field theory that captures the effects of hydrodynamic flows and viscoelasticity in channel geometries of arbitrary complexity. This method provides capabilities beyond that of previous DSCFT and GL approaches in that it allows us to study the dynamics of complex fluid systems under flow environments that were previously inaccessible and that approximate realistic processing conditions. The incorporation of rigid wall fields in DSCFT also provides a method for measuring the force exerted on the walls, enabling rheological predictions.

We are grateful to R. Ahluwalia, K. Rasmussen, A. Moreira, E. Reister, S. W. Sides, and J. C. Nave for useful discussions. This work was supported by the National Science Foundation (DMR-0312097), LANL ASC Materials, ASC HE, and ESC grants.

---

- [1] G. H. Fredrickson, *The Equilibrium Theory of Inhomogeneous Polymers* (Oxford Press, 2006).
- [2] F. Drolet and G. H. Fredrickson, Phys. Rev. Lett. **83**, 4317 (1999).
- [3] G. H. Fredrickson, V. Ganesan, and F. Drolet, Macromolecules **35**, 16 (2002).
- [4] M. W. Matsen, Journal of Physics **14**, R21 (2002).
- [5] J. G. E. M. Fraaije, B. A. C. van Vlimmeren, N. M. Maurits, M. Postma, O. A. Evers, C. Hoffmann, P. Altevogt, and G. Goldbeck-Wood, Journal of Chemical Physics. **106**, 4260 (1997).
- [6] E. Reister, M. Muller, and K. Binder, Physical Review E **64**, 41804 (2001).
- [7] R. Hasegawa and M. Doi, Macromolecules **30**, 3086 (1997).
- [8] T. Kawakatsu, Phys. Rev. E **56**, 3240 (1997).
- [9] C. Yeung and A. Shi, Macromolecules **32**, 3637 (1999).
- [10] D. Gersappe, High Performance Polymers **12**, 573 (2000).
- [11] Y. Huo, H. Zhang, and Y. Yang, Macromolecules **36**, 5383 (2003).
- [12] H. Tanaka, Phys. Rev. E **56**, 4451 (1997).
- [13] T. Taniguchi and A. Onuki, Phys. Rev. Lett. **77**, 4910 (1996).
- [14] G. Fredrickson, Journal of Chemical Physics **117**, 6810 (2002).
- [15] J. Meerveld, Rheologica Acta **43**, 615 (2004).